

Advanced Characterization and Calphad in Design and Development of Advanced High Strength Steels



R. Veerababu, R. Balamuralikrishnan, and S. Karthikeyan

1 Introduction

1.1 Microstructure at Different Length Scales

Understanding the microstructure at different length scales plays an important role in the design and development of new alloys or improving the performance of existing alloys. The microstructure can be characterized at different levels viz., optical, scanning and transmission electron microscopies and 3D atom probe. Figure 1 shows the microstructures of high strength naval steels (HSNS) using different microscopy techniques. At optical level (Fig. 1a), the microstructure shows the presence of banding of microstructure, grain size, types of phases, e.g., ferrite and pearlite. Finer details of the phases, relatively coarse precipitates along with their chemical compositions, can be obtained in scanning electron microscopy (SEM) (Fig. 1b). At electron back scattered diffraction (EBSD) level (Fig. 1c), microstructural features like different phases, grain size and its distribution, orientation of different grains, etc. can be characterized. Very fine microstructure details like dislocations, inter- and intra-lath particles of more than 5 nm size along with their chemistry and crystal structure can be obtained from transmission electron microscopy (TEM) (Fig. 1d and e). All the above microscopy techniques provide microstructural information in the lateral direction. 3D atom probe (3DAP), with its single atom resolution, provides the microstructural information in the depth direction [1]. It helps in obtaining elemental distribution in different phases, various attributes of clusters and their evolution with processing and chemistry (Fig. 1f).

R. Veerababu (✉) · R. Balamuralikrishnan
Defense Metallurgical Research Laboratory (DMRL), Kanchanbagh, Hyderabad, India
e-mail: veera.dmrl@gov.in

R. Veerababu · S. Karthikeyan
Department of Materials Engineering, Indian Institute of Science, Bangalore, India
e-mail: karthik@materials.iisc.ernet.in

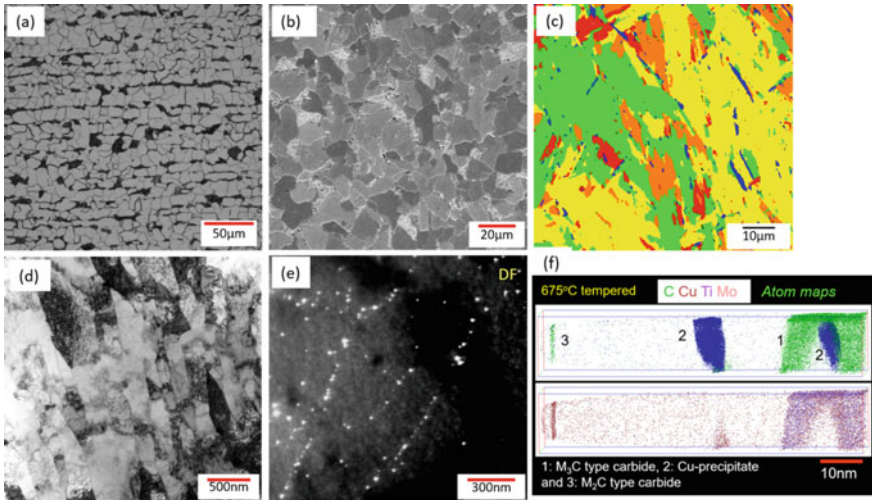


Fig. 1 Microstructure of high strength naval steels (HSNS) at different length scales; **a** optical, **b** SEM, **c** EBSD, **d** and **e** TEM and **f** 3D atom probe

If one understands the microstructure of a given material at these different levels as a function of composition and processing windows and its correlation to the obtained mechanical properties of the material, one would be able to design a new composition or processing windows or modify the existing composition to achieve improved mechanical properties. This approach for alloy design has been employed in design and development of secondary hardening ultra-high strength (SHUHS) steels through balancing of strength and fracture toughness. This book chapter describes our efforts in minimizing the number of experiments in improving the strength of existing DMRL UHS steel without compromising the toughness. Initially, a brief background (Sect. 2) on the development of typical SHUHS steels and the current understanding of the microstructure of these steels has been presented followed by recent developments in understanding the microstructure using 3D atom probe with reference to DMRL UHS steel (Sect. 3.1). Since the objective of the work is to minimize the number of experiments through thermodynamic calculations, ThermoCalc has been used extensively to understand the phase stability and its correlation to the achieved mechanical properties in typical SHUHS steels and DMRL steel. ThermoCalc findings and understanding of the microstructure in typical SHUHS steels and the DMRL steel have been used to select few alloys for experimental validation using thermodynamic calculations on DMRL steel by varying Cr and Mo contents and are presented in Sects. 3.2, 3.3, 3.4, 3.5, 3.6, and 3.7. Finally, before presenting the conclusions of the present work in Sect. 5, the opportunities and challenges associated with the use of semi-empirical approach in alloy design have been presented in Sect. 4.

Table 1 Nominal composition and mechanical properties of standard SHUHS steels

Steel	C	Co	Ni	Cr	Mo	Fe	Mechanical properties		
							YS, MPa	UTS, MPa	K _{IC} , MPa \sqrt{m}
HY180	0.10	8.0	10.0	2.00	1.00	Bal	1250	1380	233
AF1410	0.16	14.0	10.0	2.00	1.00	Bal	1533	1675	158
Aermet100	0.24	13.4	11.5	3.00	1.20	Bal	1724	1965	126
Aermet310	0.25	15.0	11.0	2.40	1.40	Bal	1896	2172	71
Aermet340	0.33	15.6	12.0	2.25	1.85	Bal	2068	2379	37

2 Background

2.1 Secondary Hardening Ultra-High Strength (SHUHS) Steels

SHUHS steels possess excellent combination of high strength, fracture toughness and stress corrosion cracking resistance, which make them candidate materials for niche applications such as aircraft landing gear and armor [2]. Table 1 shows the composition and mechanical properties of the standard SHUHS steels in typical heat treatment conditions [3]. Chronologically, the standard SHUHS steels have been developed in the order: HY180, AF1410, AerMet100, AerMet310 and AerMet340. It can be seen that, except for Cr, amounts of all other alloying elements have been increased progressively from HY180 to AerMet340 steels. Cr has been increased to 3wpct in AerMet100, decreased to ~2wpct and maintained in the vicinity of 2wpct in the later grades of steels. Mo and C have shown a continuous increase from HY180 to AerMet340 steel. Co was increased significantly from HY180 to AF1410 and maintained at that level in the later grades, while Ni was increased steadily from HY180 to AerMet340. With increase in the amount of total alloying elements from HY180 to AerMet340, strength properties have also been increased with concomitant decrease in fracture toughness.

2.2 Tempering Response of SHUHS Steels

The microstructure of these steels in the as-quenched condition consists essentially of lath martensite along with small amounts of undissolved primary carbides such as MC, M₆C and M₂₃C₆ [4, 5]. The typical tempering behavior of these steels (Fig. 2) reveals that [4, 6–11] during low temperature tempering (200–300 °C), the strength of the steel drops slightly with an increase in tempering temperature, it increases to reach a peak in the range 450–600 °C and tempering beyond this temperature results in a decrease in strength/hardness. In contrast, toughness increases marginally in the 200–300 °C tempering range, decreases to a minimum in the vicinity of 425 °C and

increases significantly when tempered beyond 425 °C. The toughness minimum at 425 °C has been attributed to the formation of coarse cementite (Fig. 3a). Tempering beyond 425 °C, typically in the range 450–600 °C, results in the dissolution of this coarse cementite and provides carbon for the formation of fine dislocation nucleated M_2C alloy carbides, which is associated with the peak hardness/strength of these steels. At even higher tempering temperatures, needle-shaped M_2C precipitates begin to coarsen resulting in a slight loss of strength but accompanied by a disproportionate increase in toughness (Fig. 3b). For this reason, all secondary hardening steels are put into service in this slightly overaged condition.

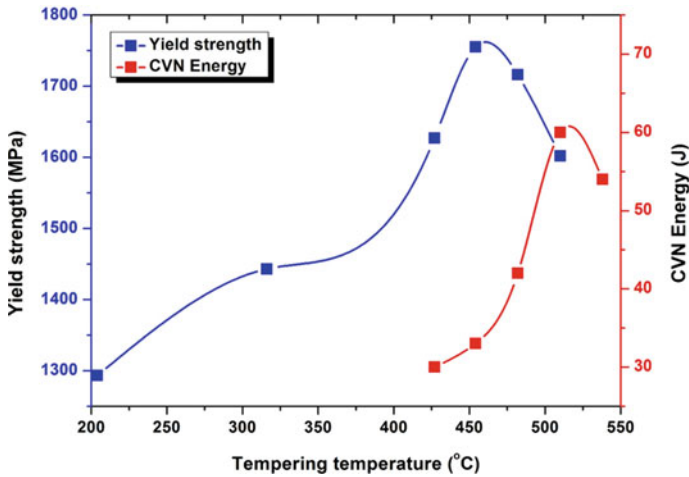


Fig. 2 Tempering response of AerMet100 steel [4]

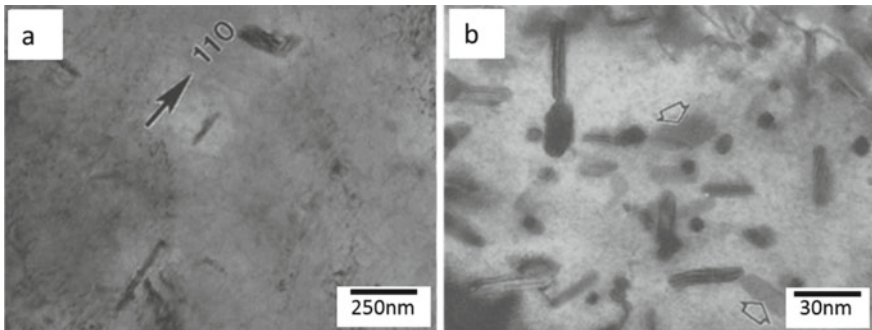


Fig. 3 TEM micrographs of Aermet 100 steel at **a** 427 °C and **b** 566 °C tempering treatments [4]

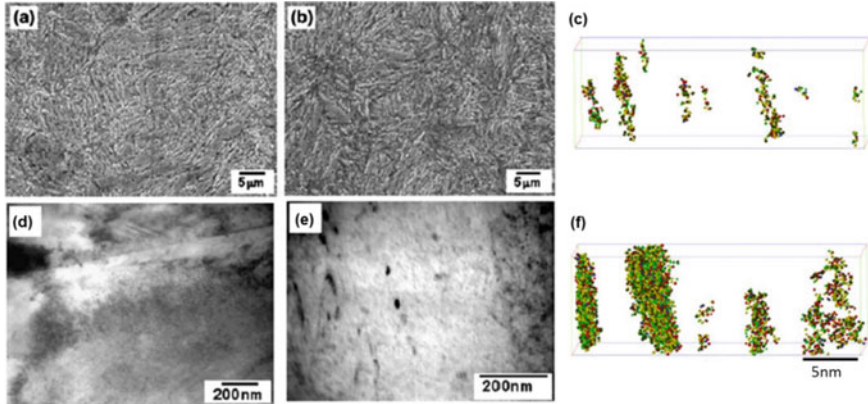
3 Recent Developments and Current Status

3.1 DMRL UHS Steel

Steel similar to typical SHUHS steels, designated as DMRL UHS steel, is being developed at DMRL with a nominal composition (in wt. %) of 0.37C, 14.8Co, 13.7Ni, 2Cr, 1Mo and Fe (bal.). Typical mechanical properties in different heat treatment conditions are shown in Table 2. This table shows that at similar strength levels, the samples tempered for 8 h at a given tempering temperature of either at 485 °C or 495 °C show nearly 50% improvement on fracture toughness. Microstructural characterization at SEM (Figs. 4a and b) and TEM (Figs. 4d and e) scales shows no apparent differences, and differences in cluster size and number density have been observed in 3D atom probe (Figs. 4c and f). The sample tempered for 8 h shows significantly higher fraction of clusters compared to 4 h sample. It has been reported that clusters have the potential to significantly improve both strength and toughness simultaneously [12, 13]. In addition to this, significant fractions of clusters were found to be deficient in carbon along with clusters close to M_2C stoichiometry [14]. To understand the influence of composition on the amount of M_2C and the presence of carbon-deficient clusters, composition of M_2C has been examined—to form M_2C , two metal atoms (Cr, Mo and V) and one carbon atom are required. DMRL SHUHS steel contains (in at. %) 2.16Cr, 0.58Mo, 0.22 V and 1.73C. The total amount of carbide forming elements (Cr + Mo + V) is 2.96at. %. If we assume that the entire amount of carbide forming elements are consumed in forming M_2C carbides, it would have only used up 1.48at. % C, resulting in the availability of excess 0.25at. % C. Moreover, in spite of the availability of this excess carbon, carbon-free clusters consisting of Cr, Mo and Fe have been observed in DMRL SHUHS steels [14]. This loss of M to such clusters results in a lesser fraction of M_2C than is possible if all available carbide forming M elements were used to form M_2C . In contrast, in standard SHUHS steels as summarized in Table 1, there is excess amount of carbide forming elements and hence increased strength. Therefore, it is hypothesized that by increasing the amount of carbide forming elements (Cr and Mo), one may be able to utilize all the excess carbon and maximize the amount of M_2C and perhaps increase strength further. This understanding has been utilized as the basis for modification of the composition of DMRL UHS steel. The question then arises as to how much the amount of Cr and Mo can be increased over and above the levels of DMRL UHS steel. It is well known that experimental design of alloys following empirical trial and error approaches, particularly of the multi-component steels containing 6–10 alloying elements, is rather expensive, time consuming and involves enormous efforts before realizing a promising composition with desired set of mechanical properties. Therefore, a semi-empirical approach involving both computations using ThermoCalc [15] and experiments has been adopted in this work.

Table 2 Mechanical properties of the DMRL SHUHS at different tempering temperatures

Heat treatment condition (Temp., °C/time)	Yield strength, MPa	UTS, MPa	Elongation, %	K_{IC} , MPa \sqrt{m}
485/4 h	1855	2105	12.6	45.0
485/8 h	1825	2040	13.4	66.0
495/4 h	1825	2050	14.0	60.5
495/8 h	1775	2030	15.0	87.0

**Fig. 4** Microstructure of DMRL UHS steel tempered at 485 °C for—4 h **a** SEM, **d** TEM and **c** atom map of clusters and—8 h **b** SEM, **e** TEM and **f** atom map of clusters

3.2 Validation of ThermoCalc for Design of SHUHS Steels

Initially, ThermoCalc has been used to predict the equilibrium phase fractions and their compositions as a function of temperature in typical SHUHS steels for which experimental data is available. These calculations suggest that ThermoCalc can be used to investigate phase equilibria in standard SHUHS steels, especially if corrections are made by suppressing the stable carbide phases that are typically not observed experimentally for kinetic and other reasons. A typical phase fraction calculation depicting the comparison of M_2C phase fraction in standard SHUHS steels as a function of temperature in the tempering regime is shown in Fig. 5. The predicted maximum amount of M_2C increases (in mole %) from ~1.4 in HY180 to 2.3 in AF1410 and further to 3.4 in AerMet100. The temperature at which complete dissolution of a given precipitate occurs is called the maximum dissolution temperature, T_d , and this temperature also follows the same trend, i.e., increasing from 740 °C in HY180 to 770 °C in AF1410 to 825 °C in AerMet100. The higher mole fraction and T_d for M_2C in AF1410 steel may be attributed to higher carbon content in AF1410 relative to HY180 (Table 1). The amount of M_2C in AerMet100 steel is significantly higher than the other two due to higher amounts of all carbide forming

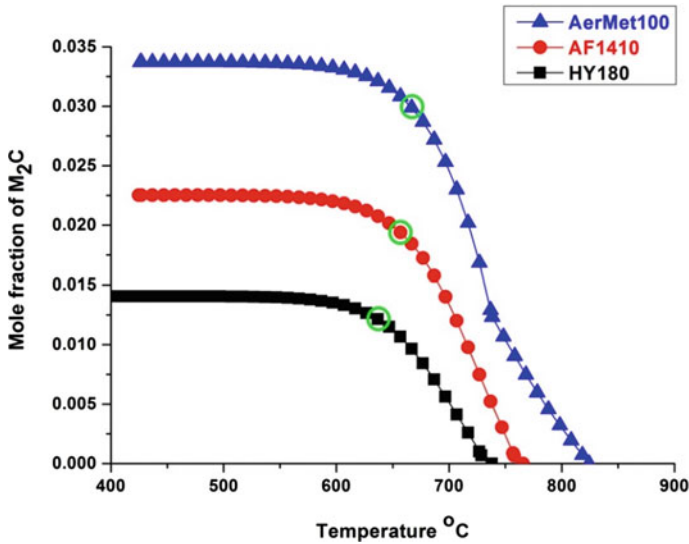


Fig. 5 M_2C phase fraction in standard SHUHS steels as a function of temperature in the tempering regime

elements (Table 1). It can be seen from Fig. 5 and Table 1 that the predicted M_2C phase fractions of the steels correlate well with the observed mechanical properties: AerMet100 with highest M_2C carbide fraction exhibits the highest strength. This suggests that if one were to design a new alloy with enhanced strength, one could do so by increasing the amount of M_2C carbides, which in turn could be achieved by modifying the composition.

3.3 Calculations Based on DMRL UHS Steel

Based on the understanding of the ThermoCalc predictions in standard SHUHS steel, similar calculations have been extended to DMRL UHS steel through variations of Cr and Mo and keeping the other alloying elements same as those in DMRL steel except Fe. Contour plots of M_2C phase fraction and Cr/Mo ratio in M_2C carbide at a typical tempering temperature of 450 °C are shown in Fig. 6. The reason for mapping the Cr/Mo ratio of M_2C carbide is that this ratio influences the coarsening resistance of the carbide during tempering and it is desirable to keep this ratio at minimum to obtain maximum coarsening resistance for the M_2C carbide and hence higher strengthening [16, 17]. DMRL composition is indicated with dark spot in both these maps. The most desirable region in the phase fraction map (Fig. 6a) is red color region with maximum M_2C phase fraction and the desirable region in Cr/Mo ratio map (Fig. 6b) is gray color region.

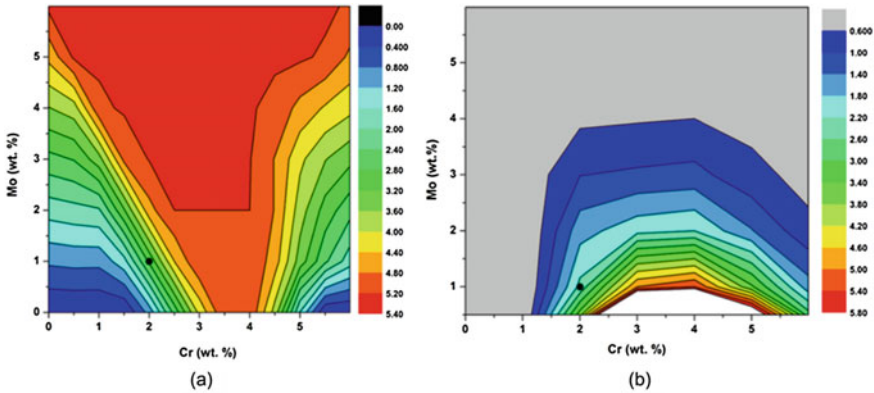


Fig. 6 Contour maps with variation of Cr and Mo in DMRL UHS steels at 450 °C; **a** M_2C phase fraction and **b** Cr/Mo ratio of M_2C carbide

3.4 Design Criteria

Initially, the M_2C fraction and Cr/Mo ratio have been considered to select the alloys. The design criteria has been arbitrarily chosen such the model alloys shall have at least 50% higher M_2C phase fraction ($\geq 4.32\%$) than the DMRL steel with 2.88 mol.% and Cr/Mo ratio of the M_2C carbide shall be at least 50% lower (≤ 1.16) than that of the DMRL steel with 2.31. Based on these two criteria, a combined contour map of M_2C fraction and Cr/Mo ratio at 450 °C tempering temperature has been plotted as shown in Fig. 7. The *maroon* color line and the horizontally hatched region in *maroon* indicate the range of compositions where the M_2C fraction is equal to lesser than the desired target ($\geq 4.32\%$). Similarly, the *green* color line and the vertically hatched region in *green* represent the range of compositions where the Cr/Mo ratio of the carbide is equal to or higher than the target (≤ 1.16). The *white* unhatched region is the most desirable region which indicates the compositions where the M_2C fraction is at least 50% higher and the Cr/Mo ratio in M_2C is at least 50% lower than that in DMRL UHS steel. Three model alloys, C_{21} , C_{23} and C_{55} , indicated with black spots, have been selected for experimental validation. The first and second subscripts denote the nominal weight percent of the Cr and Mo, respectively. Other alloying elements such as C, Co and Ni are kept at the levels of DMRL UHS steel, i.e., C: 0.37, Co: 15 and Ni: 14.

3.5 Experimental Results on Model Alloys

The selected model alloys have been melted as 500gms pancakes, rolled to 3-mm-thick sheets and subjected to a series of austenitizing treatments between 1000 and 1150 °C to optimize the austenitizing temperature [18]. These results suggest that the

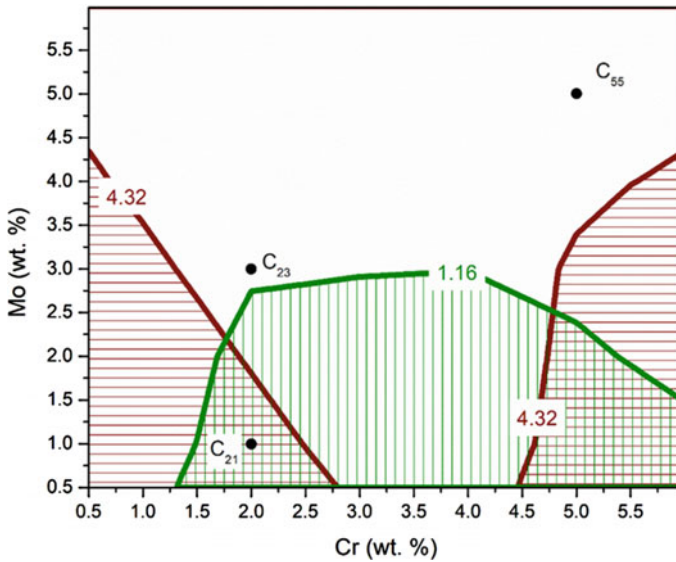


Fig. 7 Combined contour map of both M_2C fraction and Cr/Mo ratio in M_2C carbide at 450 °C with variation of Cr and Mo concentrations. The three model alloy compositions are indicated with filled black circles

hardness is relatively insensitive to austenitizing temperature when the temperature is increased from 1000 to 1150 °C, whereas the hardness is decreased in C_{23} steel and more drastically decreased in C_{55} steel with increase in austenitizing temperature. Further, it has been found that the C_{21} steel exhibited highest hardness followed by C_{23} and C_{55} in spite of higher Cr and Mo levels in the latter steels. Microstructural origin for the lower hardness in C_{23} and C_{55} steels at 1000 °C and 1150 °C at different length scales reveals the presence of higher fraction of retained austenite as shown in Fig. 8. Quantification of amount of retained austenite (RA) of samples subjected to oil quenching and LN_2 (OQ + LN_2) treatment following austenitizing using EBSD (Table 3) suggests that with increase in Cr and Mo contents and austenitizing temperature, austenite has become more stable and the fraction of RA in C_{55} steel is more than 50%. Further, it has been observed that C_{55} retained significant fraction of undissolved precipitates even after austenitizing at 1150 °C (Fig. 9). Based on these experimental results, C_{55} was not studied further since it is not fulfilling the design criteria of having maximum amount of martensite for matrix strengthening and retaining higher fraction of undissolved precipitates which minimizes the amounts of alloying elements participating in secondary hardening reaction to form strengthening precipitates and hence reducing the strength of the steel. Therefore, all the further studies were concentrated on C_{23} and compared against the C_{21} steel, being the base composition above which the composition is modified for improved performance.

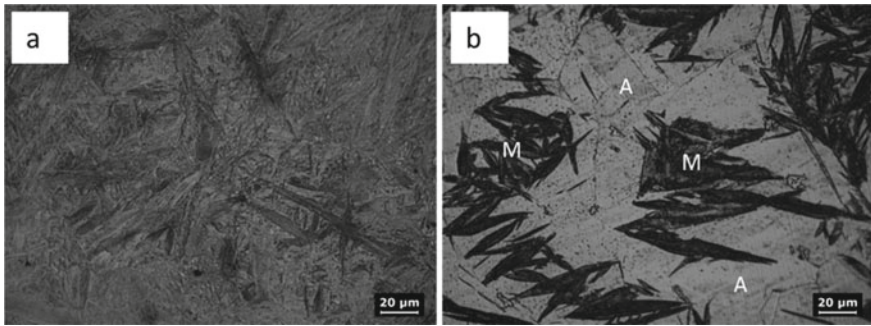


Fig. 8 Optical micrographs of samples austenitized at 1150 °C; **a** C₂₃ and **b** C₅₅

Table 3 Relative amounts of retained austenite in C₂₃ and C₅₅ subjected to austenitizing at 1000 °C and 1150 °C followed by OQ + LN₂ treatment

Steel	Austenitizing temperature, °C	Area % of austenite
C ₂₃	1000	2.08
	1150	8.69
C ₅₅	1000	40.70
	1150	56.30

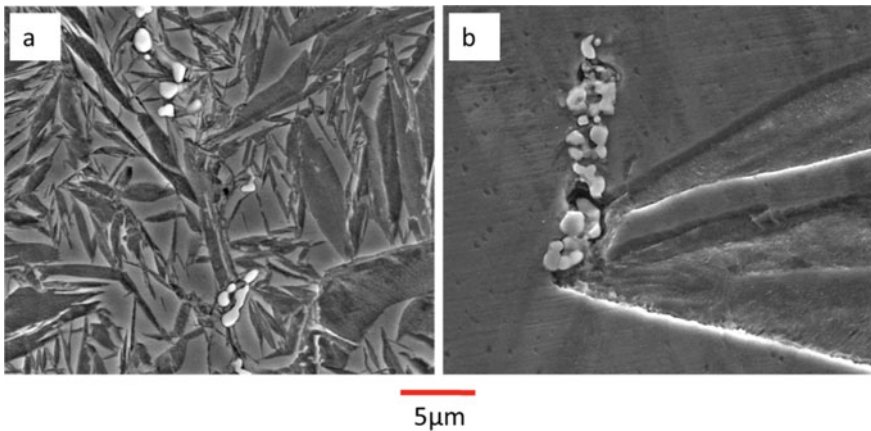


Fig. 9 SEM micrographs of samples subjected to 1150 °C, followed by OQ + LN₂ treatment; **a** C₂₃ and **b** C₅₅ [18]

3.6 Comparison of C₂₁ and C₂₃ Alloys

Both C₂₁ and C₂₃ steels exhibit similar tempering response, which shows that the hardness increases slowly at lower tempering temperatures of nearly 300 °C, reaches

a peak at 450 °C and then falls sharply when tempered at temperatures beyond 450 °C. However, the hardness of C₂₃ was found to be significantly higher than C₂₁ at all tempering temperatures, reaching a maximum difference of 90VHN at 450 °C. Detailed microstructural characterization of both C₂₁ and C₂₃ steels suggests similar microstructural features, as observed in typical SHUHS steels [4, 16, 19–24], showing the presence of alloy cementite at lower tempering temperatures of 400 °C (Fig. 10). This alloy cementite was found to be dissolved and replaced by fine M₂C carbides when tempered at tempering temperatures of above 500 °C. However, at peak aged (450 °C) and slightly over aged (500 °C) conditions, it was rather difficult to establish the type of precipitates due to fine nature of the precipitates and high dislocation density of the martensitic matrix [4, 25, 26]. 3D atom probe, with single atom atomic resolution [1], has been used to identify the nature of these fine precipitates. In these aged conditions, extremely fine precipitates and numerous atomic clusters have been observed using atom probe as shown in atom map of 450 °C tempered sample (Fig. 11). Detailed quantitative analysis of these clusters in terms of cluster composition, size, number density and volume fraction has been carried out. When the composition of these clusters in terms of (Cr+Mo)/C ratio is plotted as a function of size in the form of a contour map, three individual peaks in number density have been observed for both C₂₁ and C₂₃ steels suggesting three different types of clusters (Fig. 12) [27].

Based on the observation of three peaks and the type of carbides typically formed in this class of steels, clusters have been classified into three types, namely *Type I* (carbon-rich clusters, (Cr+Mo)/C ratio < 1.5), *Type II* (clusters close to M₂C stoichiometry, (Cr+Mo)/C ratio = 1.5–3.25) and *Type III* (metal-rich clusters, (Cr+Mo)/C ratio > 3.25). Evolution of cluster composition and volume fraction (V_f) of the clusters (Fig. 13) with aging temperature in C₂₁ steel suggest that *Type I* clusters dissolve initially to form *Type II* and *Type III* clusters at lower aging temperatures of 400 °C, and when the samples are tempered at relatively higher temperatures, *Type III* clusters also gets dissolved and are replaced by the *Type II* clusters. Cluster

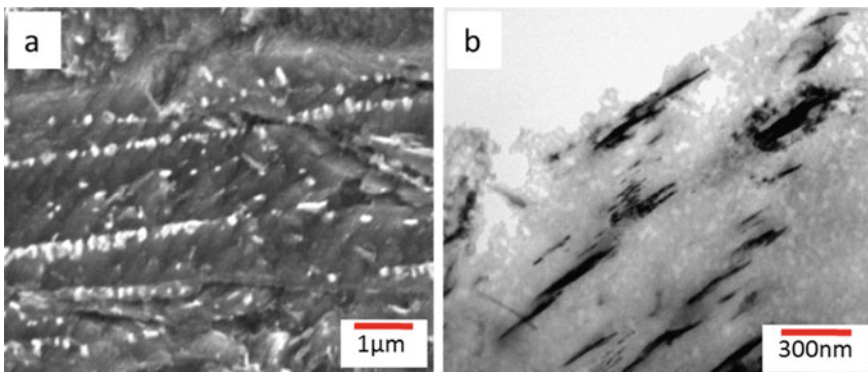


Fig. 10 Micrographs of C₂₃ steel tempered at 400 °C; **a** SEM and **b** bright field TEM image

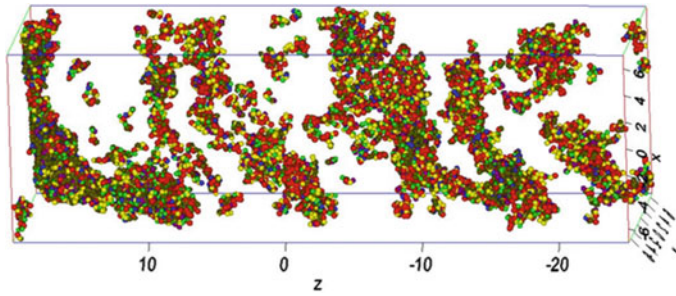


Fig. 11 Atom map showing the presence of fine precipitates and clusters in C_{23} tempered at $450\text{ }^{\circ}\text{C}$

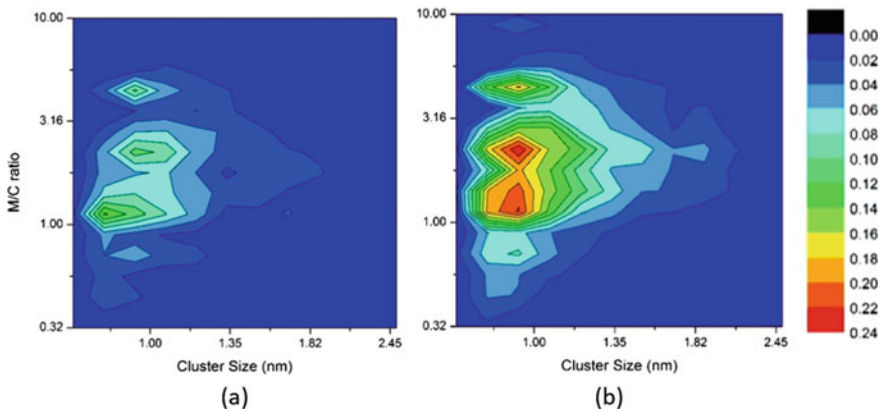


Fig. 12 Contour maps in terms of number density, $(\text{Cr}+\text{Mo})/\text{C}$ ratio and size of clusters in $400\text{ }^{\circ}\text{C}$ tempered samples; **a** C_{21} and **b** C_{23} [27]

composition evolution in C_{23} was found to be slightly different. When the samples are aged at $400\text{ }^{\circ}\text{C}$ or beyond, both *Type I* and *Type III* clusters get dissolved and replaced by *Type II* clusters. Further, C_{23} was found to contain more numerous *Type II* clusters compared to C_{21} which can be attributed to higher Mo content. In both steels, the size of *Type II* clusters has been increased with increase in aging temperature and M/C ratio of the clusters approaches close to 2 with increase in size of the clusters suggesting that these clusters are either fine M_2C carbides or precursors to the formation of M_2C carbides. Timokhina et al. [28] also reported similar results in Ti-Mo steel which suggests that the composition of Ti-Mo-Fe clusters approaches equilibrium composition of MC precipitates as the size of the clusters is increased.

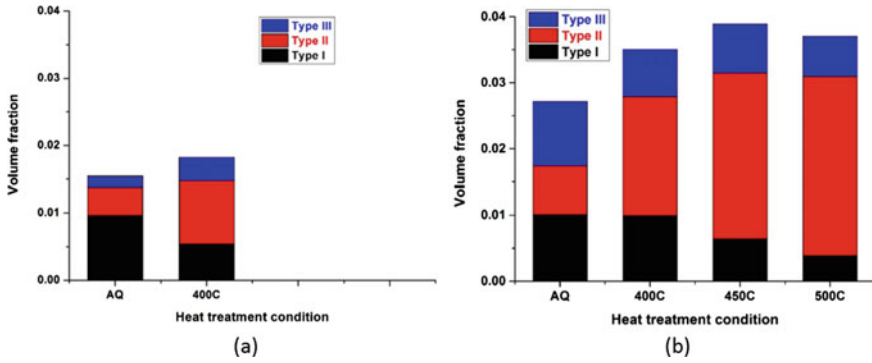


Fig. 13 Volume fraction of various types of clusters under different heat treatment conditions; **a** C₂₁ and **b** C₂₃ [27]

Table 4 Comparison of M₂C fraction and Cr/Mo ratio from ThermoCalc and 3D atom probe

Steel	Mole fraction of M ₂ C		Cr/Mo ratio	
	ThermoCalc	3DAP	ThermoCalc	3DAP
C ₂₁	2.58	0.93	2.46	0.97
C ₂₃	5.09	1.80	0.98	0.60

3.7 Comparison of ThermoCalc and Experimental Results

The observed hardness differences between C₂₁ and C₂₃ can be correlated to microstructural features, especially *Type II* clusters (M₂C type) which in turn can be attributed to higher Mo content in C₂₃ relative to C₂₁. Summary of mole fraction and Cr/Mo ratio of M₂C carbide predicted from ThermoCalc and the measured volume fraction and Cr/Mo ratio from 3DAP experiments is shown in Table 4. The predicted mole fraction of the M₂C carbide from ThermoCalc in C₂₃ is almost double that of C₂₁. 3D atom probe results also suggest that the measured volume fraction of M₂C type clusters is also double that of C₂₁. Similarly, the Cr/Mo ratio predicted by ThermoCalc and measured by 3D atom probe is close to half in C₂₃ compared to that in C₂₁. Although the absolute values of M₂C phase fraction and the Cr/Mo ratio of the M₂C carbide may not be the same in ThermoCalc predictions and 3D atom probe, the trends predicted by both theoretical calculations and experimental measurements are the same.

4 Opportunities and Challenges

The design approach adopted in this work involves understanding the existing the experimental data in the field of SHUHS steels and applying the computational tools

such as ThermoCalc for alloy designing. Though the methodology was explained with reference to SHUHS steels, the general principles elucidated here, in general, are applicable to other steels as well as other alloy systems. This approach provides ample opportunities in alloy designing. One can theoretically verify several combinations of alloying elements with varying amounts and understand the influence of these alloying elements on phase stability, amounts of phases and their composition as a function of temperature without going for experimental validation of multiple alloys. The objective of the present work is not to replace the experiments completely. Instead, design multiple alloys theoretically and experimentally process very few alloys that appear to be more promising. This approach not only reduces the number of alloys for experimental validation but also can be used to predict the processing windows for the selected alloys, which would in turn further reduce the experimental efforts. Therefore, this approach significantly reduces the more expensive experiments, saves time and efforts in developing new alloys or improving the performance of existing alloys.

Though this approach significantly reduces the experimental efforts and reduces the alloy development time, it also poses several challenges. One should have a thorough knowledge of the alloy systems in terms of formation of different phases, approximate temperature ranges for their formation and so on. For example, in the current work, M_6C and $M_{23}C_6$ are predicted as stable phases when both these phases were allowed to form in the calculations, and the strengthening precipitate in this class of steels, M_2C , has not been predicted. However, extensive literature suggests that M_2C is the strengthening precipitate in this class of steels [4, 10, 16, 19, 20]. Since M_6C and $M_{23}C_6$ are thermodynamically more stable carbides and hence were predicted in the calculations instead of meta-stable M_2C carbide. However, experimentally, M_6C and $M_{23}C_6$ normally do not form in the typical tempering regimes in these steels for kinetic reasons. Therefore, these carbides have been suppressed in the calculations. Unless one has a fair knowledge of formation of different phases in a given alloy system, there is every chance that the results can be misinterpreted. However, it is often difficult to obtain prior knowledge on all alloy systems of interest, especially in the absence of extensive experimental work. In such cases, caution must be exercised while interpreting the results predicted from the calculations.

5 Conclusions

This work has clearly demonstrated that understanding the microstructure at different length scales can play a major role in the design and development of a new set of alloys with improved performance or designing new alloys. A semi-empirical approach using ThermoCalc calculations has been employed to improve the performance of the secondary hardening ultra-high strength steels. ThermoCalc has been used to select two new alloys (C_{23} and C_{55}) based on DMRL steel with higher M_2C phase fraction and lower Cr/Mo ratio. Experimental validation of these two alloys suggests that C_{55} steel contains significant fraction of undissolved precipitates and more than 50%

austenite even after 1150 °C austenitizing treatment. Tempering studies on C₂₁ and C₂₃ reveal that C₂₃ was stronger than C₂₁ by more than 10%. Microstructural studies tempered samples at optical, SEM and TEM level reveal the presence of typical lath martensite and fine precipitates in both C₂₁ and C₂₃ steels. Advanced characterization using 3DAP suggests that C₂₃ contained a significantly higher fraction of clusters close to M₂C stoichiometry, with a lower Cr/Mo ratio than C₂₁. This is in accordance to the design objective for this alloy. Therefore, the design objective of increasing the strength of the existing DMRL SHUHS steel through alloy modifications for achieving higher M₂C fraction was realized successfully. This work has confirmed that a judicious use of ThermoCalc with an emphasis on qualitative trends can be used for designing new alloy compositions in this class of SHUHS steels.

Acknowledgements This research was funded by the Defense Research and Development Organization (DRDO), India. Dr. G Madhusudhan Reddy, OS and Director, Defense Metallurgical Research Laboratory (DMRL), Hyderabad, to publish this work is gratefully acknowledged. The authors wish to thank Dr. M. Srinivas, retired scientist from DMRL and extensively worked on UHS steels for fruitful discussions. The authors are grateful to Professor T. A. Abinandanan, former Chairman, Dept. of Materials Engg., IISC, Bangalore, Dr. K. Muraleedharan, Director (retd.), CGCRI, Kolkata, Dr. G. Malakondaiah, former Director, DMRL and former Chief Controller (HR&D) at DRDO Headquarters, Dr. S. V. Kamat, DS and former Director, DMRL and DG (NS&M) for their constant encouragement and support.

References

1. D.N. Seidman, Three-dimensional atom-probe tomography: advances and applications. *Annu. Rev. Mater. Res.* **37**, 127–158 (2007)
2. J.M. Dahl, P.M. Novotny, Airframe and landing gear alloy. *Adv. Mater. Processes* **155**(3), 23–25 (1999)
3. R. Veerababu, in *Microstructural Studies on High Cr-Mo Secondary Hardening Ultra-High Strength Steels* (Indian Institute of Science, 2015)
4. R. Ayer, P.M. Machmeier, Transmission electron microscopy examination of hardening and toughening phenomena in Aermet 100. *Metall. Trans. A* **24**(9), 1943–1955 (1993). <https://doi.org/10.1007/BF02666329>
5. M. Grujicic, Thermodynamics aided design of high Co-Ni secondary hardening steels. *Calphad* **14**(1), 49–59 (1990). [https://doi.org/10.1016/0364-5916\(90\)90039-3](https://doi.org/10.1016/0364-5916(90)90039-3)
6. K.S. Cho, J.H. Choi, H.S. Kang, S.H. Kim, K.B. Lee, H.R. Yang, H. Kwon, Influence of rolling temperature on the microstructure and mechanical properties of secondary hardening high Co-Ni steel bearing 0.28wt% C. *Mat. Sci. Eng.: A* **527**(27–28), 7286–7293 (2010). <https://doi.org/10.1016/j.msea.2010.07.069>
7. L.E. Iorio, J.L. Maloney, W.M. Garrison Jr., 40th Mechanical Working and Steel Processing Conf. Proc., ISS-AIME, Warrendale, PA, 901–920 (1999)
8. P. Machmeier, T. Matuszewski, R. Jones, R. Ayer, Effect of chromium additions on the mechanical and physical properties and microstructure of Fe-Co-Ni-Cr-Mo-C ultra-high strength steel: Part I. *J. Mater. Eng. Perform.* **6**(3), 279–288 (1997). <https://doi.org/10.1007/s11665-997-0091-3>
9. J.S. Montgomery, G.B. Olson, Proc. G.R. Speich Symp., ISS, Warrendale, PA, 177–214 (1992)
10. G.R. Speich, D.S. Dabkowski, L.F. Porter, Strength and toughness of Fe-10Ni alloys containing C, Cr, Mo, and Co. *Metall. Trans.* **4**(1), 303–315. <https://doi.org/10.1007/BF02649630>

11. H.R. Yang, K.B. Lee, H. Kwon, Effects of Ni additions and austenitizing temperature on secondary hardening behavior in high Co-Ni steels. *Metall. and Mater. Trans. A.* **32**(9), 2393–2396 (2001). <https://doi.org/10.1007/s11661-001-0213-8>
12. E.V. Pereloma, A. Shekhter, M.K. Miller, S.P. Ringer, Ageing behaviour of an Fe–20Ni–1.8Mn–1.6Ti–0.59Al (wt%) maraging alloy: clustering, precipitation and hardening. *Acta Mat.* **52**(19), 5589–5602 (2004). <https://doi.org/10.1016/j.actamat.2004.08.018>
13. A. Shekhter, H.I. Aaronson, M.R. Miller, S.P. Ringer, E.V. Pereloma, Effect of aging and deformation on the microstructure and properties of Fe-Ni-Ti maraging steel. *Metall. and Mater. Trans. A.* **35**(3), 973–983 (2004). <https://doi.org/10.1007/s11661-004-0024-9>
14. R. Veerababu, R. Balamuralikrishnan, K. Muraleedharan, M. Srinivas, Three-Dimensional Atom Probe Investigation of Microstructural Evolution during Tempering of an Ultra-High-Strength High-Toughness Steel. *Metall. and Mater. Trans. A.* **39**(7), 1486–1495 (2008). <https://doi.org/10.1007/s11661-007-9333-0>
15. B. Sundman, B. Jansson, J.-O. Andersson, The Thermo-Calc databank system. *Calphad* **9**(2), 153–190 (1985). [https://doi.org/10.1016/0364-5916\(85\)90021-5](https://doi.org/10.1016/0364-5916(85)90021-5)
16. R. Ayer, P.M. Machmeier, Microstructural basis for the effect of chromium on the strength and toughness of AF1410-based high performance steels. *Metall. and Mater. Trans. A.* **27**(9), 2510–2517 (1996). <https://doi.org/10.1007/BF02652345>
17. L.E. Iorio, in *The Effect of Increasing Carbon Level on Titanium Carbosulfides and Their Influence on Toughness in Ultra-high Strength Steels*, 5–10 (Carnegie Mellon, 2000)
18. R. Veerababu, K. Satya Prasad, S. Phani, K., Balamuralikrishnan, S. Karthikeyan, Austenite stability and M2C carbide decomposition in experimental secondary hardening ultra-high strength steels during high temperature austenitizing treatments. *Mater. Charact.* **144**, 191–204 (2018). <https://doi.org/10.1016/j.matchar.2018.07.013>
19. H. Kwon, J.H. Lee, K.B. Lee, C.M. Kim, H.R. Yang, Effect of alloying additions on secondary hardening behavior of Mo-containing steels. *Metall. and Mater. Trans. A.* **28**(3), 621–627 (1997). <https://doi.org/10.1007/s11661-997-0047-0>
20. H. Kwon, J.H. Lee, K.B. Lee, H. Kwon, C.M. Kim, H.R. Yang, Effects of Co and Ni on secondary hardening and fracture behavior of martensitic steels bearing W and Cr. *Metall. and Mater. Trans. A.* **29**(1), 397–401 (1998). <https://doi.org/10.1007/s11661-998-0191-1>
21. H.M. Lee, S.M. Allen, Coarsening resistance of M2C carbides in secondary hardening steels: Part III. Comparison of theory and experiment. *Metall. Trans. A.* **22**(12), 2877–2888 (1991). <https://doi.org/10.1007/BF02650249>
22. H.M. Lee, S.M. Allen, M. Grujicic, Coarsening resistance of M2C carbides in secondary hardening steels: Part I. Theoretical model for multicomponent coarsening kinetics. *Metall. Trans. A.* **22**(12), 2863–2868 (1991a). <https://doi.org/10.1007/BF02650247>
23. H.M. Lee, S.M. Allen, M. Grujicic, Coarsening resistance of M2C carbides in secondary hardening steels: Part II. Alloy design aided by a thermochemical database. *Metall. Trans. A.* **22**(12), 2869–2876 (1991b). <https://doi.org/10.1007/BF02650248>
24. K.B. Lee, H. Kwon, H. Kwon, H.R. Yang, Secondary hardening and impact fracture behavior in isothermally aged Mo, W, and Mo-W steels. *Metall. and Mater. Trans. A.* **32**(7), 1862–1866 (2001). <https://doi.org/10.1007/s11661-001-0163-1>
25. J. Akre, F. Danoix, H. Leitner, P. Auger, The morphology of secondary-hardening carbides in a martensitic steel at the peak hardness by 3DFIM. *Ultramicroscopy* **109**(5), 518–523 (2009). <https://doi.org/10.1016/j.ultramicro.2008.11.010>
26. K. Stiller, L.-E. Svensson, P.R. Howell, W. Rong, H.-O. Andrén, G.L. Dunlop, High resolution microanalytical study of precipitation in a powder metallurgical high speed steel. *Acta Metall.* **32**(9), 1457–1467 (1984). [https://doi.org/10.1016/0001-6160\(84\)90092-0](https://doi.org/10.1016/0001-6160(84)90092-0)
27. R. Veerababu, R. Balamuralikrishnan, S. Karthikeyan, Nanoscale clusters in secondary hardening ultra-high strength steels with 1 and 3 wt% Mo: An atom probe investigation. *J. Mater. Res.* **35**(14), 1763–1776 (2020). <https://doi.org/10.1557/jmr.2020.145>
28. I. Timokhina, M.K. Miller, J. Wang, H. Beladi, P. Cizek, P.D. Hodgson, On the Ti-Mo-Fe-C atomic clustering during interphase precipitation in the Ti-Mo steel studied by advanced microscopic techniques. *Mater. Des.* **111**, 222–229 (2016). <https://doi.org/10.1016/j.matdes.2016.08.086>